Experimental Analysis for Modeling Color of Halftone Images

G.M. Atiqur Rahaman[1(✉)], Ole Norberg[2], and Per Edström[1]

[1] Department of Natural Sciences, Mid Sweden University, Örnsköldsvik, Sweden
gmatiqur@gmail.com, per.edstrom@miun.se
[2] Department of Applied Physics and Electronics, Umeå University, Umeå, Sweden
ole.norberg@umu.se

Abstract. Reflectance models such as the monochrome Murray–Davies (MD) and the Neugebauer color equations make inaccurate predictions owing to changes in reflectance or tristimulus values (TSVs) of halftone dots and the paper between the dots. In this paper, we characterize the change of micro-TSVs as a function of printed area in spectral halftone image by a power function and compare its prediction efficiency using theoretically and experimentally measured limiting TSVs assuming dots of uniform thickness. We found that experimentally accounting for dot thickness variations as solid and mixed areas more precisely explained the single-model parameter that captured the observed lateral light scattering effect. The results showed that incorporating empirically modeled TSVs of the dots and the paper between dots, as well as introducing a new term addressing mixed area in the MD equation, produced CIE ΔE^*_{ab} in the range 1.22–1.76, and the overall gain was more than 1 ΔE^*_{ab}.

Keywords: Spectral image · Halftone · Color · Light scattering · Murray-Davies

1 Introduction

In printing, the surface coverage of ink is varied to reproduce different tones or lightness levels in a halftone image. A halftone reflection prediction model establishes the correct relation between the reflectance of printed surfaces and the amount of printed ink to render the reproduction system reliable [1]. The prediction is mainly made by using the measured average reflectance of a set of halftone patches. Successful models account for the observed effect because of lateral light scattering within the substrate as a function of printed dot coverage. Furthermore, accounting for the ink-spreading effect generates more accurate results. However, currently available empirical models find the connection to the classical Murray–Davies (MD) model for monochrome [2] because the MD model is theoretically successful in establishing a linear relation between the fractional coverage of fulltone ink (a) and the average reflectance of the halftone image by assuming uniform thickness and constant reflectance of the ink and the paper, as follows:

$$R_{halftone} = a\, R_{ink} + (1 - a)\, R_{paper} \tag{1}$$

A. Trémeau et al. (Eds.): CCIW 2015, LNCS 9016, pp. 69–80, 2015.
DOI: 10.1007/978-3-319-15979-9_7

In principle, the formula represents the conservation of energy by summing up all light reflected off the components. In practice, this equation predicts values different from the actual values because of mechanical and optical dot gains. The following correction was subsequently made to the equation by adding an empirical factor, known as the Yule–Nielsen *n-value,* to account for the optical dot gain [2]:

$$R_{halftone}^{1/n} = a\, R_{ink}^{1/n} + (1 - a)\, R_{paper}^{1/n} \tag{2}$$

The *n-value* improves prediction accuracy but explains light interactions for only a limited class of cases [3]. Furthermore, the linearity of the MD model is lost. This can be traced to the false assumption of the constant reflectance of the ink and the paper over the entire surface. Internal changes in reflectance values were subsequently characterized mathematically by an additional parameter to account for the effect of variations in colorimetric values surrounding the dot boundary [4]. Modification was made to Eq. 1 by retaining its original form but accommodating variable reflectances [4].

P.G. Engeldrum empirically studied changes in the reflectance of dots and the paper between dots in halftone prints, and reported results in terms of the International Commission on Illumination's (CIE) tristimulus values (TSVs) [5]. He showed that paper TSVs are linear mixtures of plain paper and a limiting TSV, whereas dot TSVs are linear mixtures of fulltone ink and the same limiting TSV. The limiting TSV refers to the TSVs of the paper when the dot coverage approaches 1.0 or the TSVs of the dots when the coverage approaches zero. The limiting value was theoretically calculated as identical to the product of the reflectance of the paper and the spectral transmittance of the ink [4, 5]. If T represents the TSV (X, Y, or Z), T_{limit} the limiting TSV, and p represents the exponent, the equations proposed by Engeldrum to characterize the changes of the TSVs of the paper and the dots, respectively, are as follows:

$$T_{pap}(a) = (T_{paper} - T_{limit})\,(1 - a)^p + T_{limit} \tag{3}$$

$$T_{dot}(a) = T_{limit} - (T_{limit} - T_{ink})\, a^p \tag{4}$$

Eq. 1 was modified to incorporate these changes as a function of fractional coverage to calculate the average tint of the halftone image as formulated in Eq. 5:

$$T_{halftone}(a) = a\, T_{dot}(a) + (1 - a)\, T_{pap}(a) \tag{5}$$

The accuracy of Eqs. 3-4 is determined by the accuracy of fitting the exponent p to the measured data. The parameter p is described in order to capture the light scattering effect as a function of paper light spread function, dot geometry, and screen frequency. However, P.G. Engeldrum assumed ink dots of uniform thickness, and the results were based on halftone prints of low screen frequency [5]. However, we show in the current study that a numerically calculated T_{limit} does not optimally fit the data for medium or high screen frequency.

In a previous study [6], we reported using experimental image analysis that effective dot area in a single-ink halftone image consists of a solid ink area and a mixed area. Solid ink refers to the dot part close to fulltone density, and mixed area refers to the periphery or edge of the dot, where ink thickness varies and light diffusion adds

blurriness. Due to variation in reflectance values in these two parts, we proposed in [6] an extension of Eq. 1 (formulated in Eq. 6 in TSV) to adjust the amount of lights, primarily assuming constant reflectance of fulltone ink and paper:

$$T_{halftone} = a_{paper}\, T_{paper} + a_{solid}\, T_{solid} + a_{mix}\, T_{mix} \tag{6}$$

The contribution of the current study is twofold. First, to the best of the author's knowledge, this study is the first to characterize changes of color in the mixed area, in addition to those in the paper and the solid ink, by analyzing single-colorant halftone microscale spectral images. Second, the accuracy of the extended MD halftone model is studied by incorporating variable colorimetry and preserving the law of conservation of energy that is suitable for explaining the physics behind the formula. Cyan, magenta, and yellow inks on two types of paper with different screen frequencies for the same printing technology are analyzed. The limiting case is measured separately for paper and dots, and the effects of solid ink as well as the mixed area are analyzed using Eqs. 3-6. The crucial parameter, i.e., the model exponent, and the relevant accuracies of the modified MD model are reported in terms of CIE ΔE^*_{ab}.

The research here is motivated to gain greater insight into the interactions between halftone ink, paper, and light, and a linear model is chosen for this background study in support with the principle of conservation of energy. A microscopic analysis should allow us to systematically discover the relevant parameters, properly relate them, and to formulate the ultimate predictions with more subtle explanations of the nonlinearity. This advanced understanding can help to improve state-of-the-art spectral printing systems incorporating the variations of the colorimetry of the paper and the ink in existing models that characterize multichannel printers.

2 Materials and Methods

2.1 Samples

A sequence of halftone patches of cyan, magenta, and yellow ink was printed on coated and uncoated papers of different optical and surface properties. The range of ink surface coverage was 0%, 3%, 10%, 20%, ..., 90%, 95%, and 100%. The halftone screen frequency was 175 *lpi* for coated paper and 144 *lpi* for uncoated paper, as is suitable for optimized print and color quality. Rotated screen amplitude modulated (AM) halftone cell produced ink dots to form the image structure on the paper.

The thickness and grammage values of the coated and uncoated paper were 0.12 mm and 150 gsm, and 0.22 mm and 200 gsm, respectively. The samples were printed using a commercial prepress printer (*HP indigo 5000*) that used liquid electrophotographic ink to produce images with sharp edges, uniform gloss, and thin layers.

2.2 Measurements

A microscopic spectral camera system was used to capture the images of halftone dot patterns and to perform measurements at the pixel level. The measurements required

in this study for each colorant were: (1) the microspectral reflectance of the solid ink, the mixed area, and the paper between the dots, (2) the corresponding fractional ink coverages, (3) the overall reflectance of halftone tints, and (4) the transmittance of the dots. The imaging setup consisted of a microscope (*Nikon Eclipse MA200)* with a CRi Nuance spectral camera attached to it. The ring-shaped illumination from the halogen lamps approximately made an 8^0 angle, whereas the detection angle was 0^0. The spatial resolution given the chosen objective was approximately 1 μm and the captured area was approximately 1 mm × 1.3 mm. The spectral resolution of the camera varied from 420 nm to 700 nm in increments of 10 nm, its bit depth was 12, and all images were directly stored as radiance images.

The spectral reflectance of each pixel was obtained by dividing the spectral radiance image by the spectral radiance image of a reference white (Spectralon Standard), and the values were multiplied by the known reflectance factors of the reference. The square root of the measured reflectance value of the fulltone image divided by the reflectance of the bare paper gave the transmittance value of the ink. Pixel reflectance was classified into that of the paper, the mixed area, and the solid ink based on the segmentation of the corresponding RGB image. The RGB image was captured at the same time and under the same conditions as the spectral radiance images. The segmentation results were also used to calculate respective fractional coverage as the ratio of the corresponding number of pixels to the total number of pixels in the image.

For segmentation, the RGB image was first converted to CMY(K) space because cyan, magenta, and yellow ink in the corresponding space provide the best contrast with the paper. The segmentation technique was based on hierarchical cluster analysis [7], which calculated two optimal threshold values to segment the gray-level image into three regions. The dynamic threshold selection technique began with the assumption that each nonempty gray level of an image histogram was a cluster. Following this, clusters closest to one another were merged together in the next level; this continued up to three levels. The mean and variance values of existing clusters and clusters formed after the possible merging operation were used to measure the distance of cluster center. The highest gray-level values in the three remaining clusters at the end of the iterative merging process were chosen as the optimal threshold values. The details of the mathematical formulation and the calculation are provided in [8, 9].

3 Results

The segmented images were used as masks to collect reflectance spectra from the corresponding spectral image. The mean spectrum of each class defined the characteristic spectral reflectance of the relevant area type. The reflectance spectra were converted to TSVs for D50 illumination and 1931 standard observers. The measured micro-TSVs of the dots and the paper between the dots as a function of printed coverage for the coated paper are shown in the *xy*-chromaticity diagram in Fig. 1. The coordinates of the theoretical limit represent TSVs of the paper when the fractional area approaches 1.0 or those of the dots when the fractional area approaches zero [5]. The chromaticity values of the paper between the dots are close to those of the bare paper, which is represented by the central convergent point that connects the limit through a

straight line. The chromaticity values of the dots are at the other end of the graph. According to [5], all dot chromaticity values should lie between the limit and the fulltone, but the chosen set of samples did not exhibit this behavior because the limiting case crossed a few dot coverages. Nevertheless, the results of the linear mixtures of TSVs [5] for both the paper and the dots are still valid because their chromaticity values fall on a line connecting the bare paper or fulltone ink to the limit.

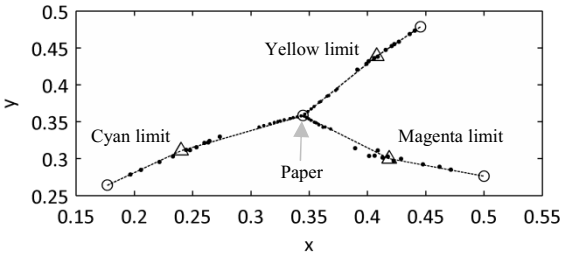

Fig. 1. CIE *xy*-chromaticity coordinates of white paper and fulltone ink (circles), paper between ink dots and fractional inks (dots), and the theoretical limits (triangles)

3.1 Full Dots and the Theoretical Limit

A nonlinear least-squares optimization technique was applied in order to fit Eqs. 3-4 to the measured data shown in Fig. 1. The performance of the characterization technique to predict TSVs as a function of fractional coverage is shown for the paper between the dots as well as for the dots in Figs. 2 and 3, respectively. The data points represent the measured CIE X, Y, and Z micro-TSVs and the lines through the points represent the predicted values. The TSVs of the paper between the dots at coverage 1.0 are the limiting values shown in the plots. Because of high color variation in the paper between the cyan and magenta dots, the predictions were not as good as for the yellow dots. Note the impact on prediction performance of a distracted data point for the cyan ink in Fig. 3.

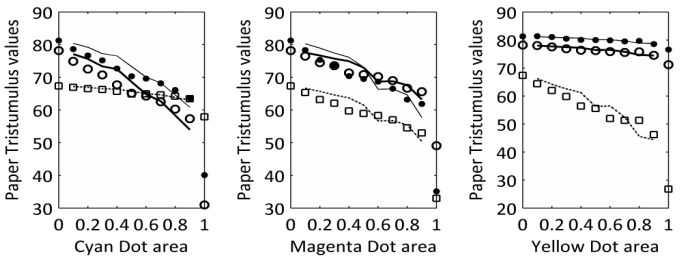

Fig. 2. The CIE X (circles), Y (dots), and Z (squares) TSVs of coated paper between the dots as a function of dot area. The lines represent the predicted values.

Table 1 lists all parameters fitted to the data for coated paper. The paper exponent was correlated with the light spread function of the paper. The exponent p to account for light scattering varied between 0.172 and 0.262, with an average value of 0.216 (root mean square (*rms*) error 1.65). For uncoated paper, the value of p ranged from 0.660 to 1.20, with an average value of 0.590 (*rms* error 2.88). However, the dot exponent p recorded notably higher values such that the average value of p was 10.5 (*rms* error 2.76) for the coated paper and 7.17 (*rms* error 2.54) for the uncoated paper.

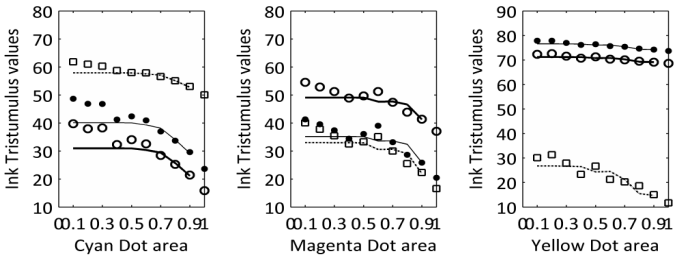

Fig. 3. The CIE X (circles), Y (solid dots), and Z (squares) TSVs of ink dots on coated paper as a function of fractional coverage. The lines represent the predicted values.

The average dot exponent p was consistently largest for cyan dots and lowest for yellow dots depending on the magnitude and uniformity of TSV changes as a function of printed area (Fig. 3). Although p was described in [5] as the parameter to capture the complex interaction of light as a function of paper spread function and halftone cell frequency, the large dot exponent value in this study indicates that it may also reveal spatial variations in reflectance around the dot edge as an effect of ink spread, absorption, and light diffusion.

Table 1. Parameters of power function fittings to the data (coated paper)

		Paper between dots					Dots			
		T_{pap}-T_{limit}	T_{limit}	p	*rms* error		T_{limit} – T_{dot}	T_{limit}	p	*rms* error
Cyan	X	47.21	30.96	0.202	2.82		15.14	30.95	15.06	4.66
	Y	41.19	40.08	0.193	2.29		16.45	40.07	14.18	4.42
	Z	9.44	57.90	0.172	0.44		7.85	57.89	14.63	1.87
Magenta	X	29.11	49.05	0.217	2.01		12.04	49.05	11.85	2.79
	Y	46.15	35.12	0.215	3.35		14.68	35.12	12.58	3.46
	Z	34.38	32.96	0.205	2.28		16.39	32.96	10.72	3.55
Yellow	X	6.98	71.19	0.238	0.56		2.58	71.18	5.21	0.66
	Y	4.70	76.56	0.242	0.36		2.89	76.56	5.01	0.68
	Z	40.59	26.75	0.262	3.27		15.06	26.75	5.27	2.81

Table 2 lists the prediction accuracy of average halftone tints in terms of CIE ΔE^*_{ab} calculated by the modified MD equation (Eq. 5) proposed in Ref. [5]. This data also serves as a metric of goodness for the fitting procedure. However, the average prediction error was lowest for cyan ink even though the data-fitting error for it was the largest. Therefore, Eq. 5 should be corrected for better explanation, and prediction accuracy of overall halftone tints.

Table 2. Prediction performance of the halftone model (Eq. 5) in terms of average CIE ΔE^*_{ab}

	Uncoated Paper		Coated Paper	
	Average	Maximum	Average	Maximum
Cyan	1.94	2.91	1.32	2.33
Magenta	3.86	7.89	2.95	7.15
Yellow	2.49	4.68	2.83	7.09

3.2 Full Dots and Measured Individual Limits

The TSVs of the paper between the dots given 99% coverage (reference 95%) and of the dots given 2.4% coverage (reference 3%) were measured and considered as limiting cases for the paper and the dot (Fig. 4). For comparison, the theoretical limit was also calculated numerically. Fig. 4 shows that the measured limits were close to one another, but at a notable distance from the theoretical value.

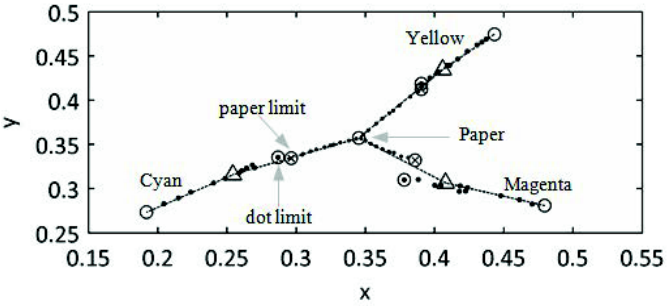

Fig. 4. CIE *xy*-chromaticity coordinates of measured paper limit (circled crosses), the dot limit (circled dots), and the theoretical limit (triangles)

The same optimization procedure was applied to fit the same set of measured data but with distinct measured limits. Table 3 lists the parameters fitted to the measured data. The use of measured limits improved the prediction accuracy of both the dot and the paper TSVs in comparison with the theoretical limit in terms of *rms* difference. Fig. 5 compares the difference in the characterization performances as a function of the limits.

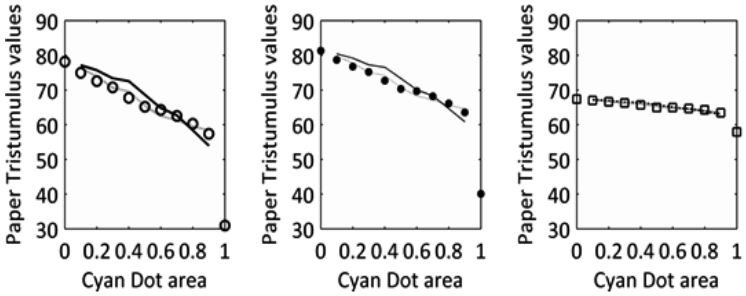

Fig. 5. Measured and predicted CIE X (circles), Y (dots), and Z (squares) TSVs of paper between the ink dots. The lines represent the predicted values (gray line: measured limit).

The exponent increased for the paper and significantly decreased in value for the dots, suggesting a dependency of the exponent on the limiting value. Note the drastic changes, especially in the value of the dot exponent p. Its value for coated paper ranged from 2.01 to 4.97, with an average of 4.08 (rms error 2.33), and that for uncoated paper ranged from 1.13 to 4.75, with an average of 2.37 (rms error 1.86). The value of p for the paper varied between 0.58 and 1.05, with an average of 0.83 (rms error 1.01) for the coated paper, and between 0.76 and 2.14, with an average of 1.25 (rms error 1.47), for uncoated paper.

Table 3. Parameters of power function fittings to the data (coated paper) with measured limits

		Paper between dots					Dots			
		T_{pap}-T_{limit}	T_{limit}	p	*rms* error		T_{limit}–T_{dot}	T_{limit}	p	*rms* error
Cyan	X	20.82	57.34	0.84	1.22		23.90	39.71	4.94	2.77
	Y	17.70	63.56	0.81	0.99		25.04	48.67	4.91	2.89
	Z	3.90	63.43	0.71	0.22		11.76	61.80	4.63	1.48
Magenta	X	12.58	65.58	0.97	1.16		17.50	54.51	4.97	2.86
	Y	19.41	61.85	1.05	1.81		20.82	41.27	5.60	3.62
	Z	14.39	52.94	0.94	1.33		23.47	40.04	4.58	3.85
Yellow	X	3.67	74.49	0.73	0.37		3.67	72.28	2.19	0.45
	Y	2.72	78.54	0.58	0.30		4.20	77.88	2.01	0.43
	Z	21.16	46.17	0.87	1.72		18.3	30.07	2.95	2.64

Table 4 reports improvements over the results listed in Table 2 for evaluating the modified MD equation (Eq. 5). Although the measured limits improved the characterization of internal changes of micro-TSVs, note that prediction of average TSVs of the halftone patch was not remarkably different (Table 4). Even overall prediction accuracy decreased for cyan and magenta colorants for the coated paper. This result also indicates that the modified MD equation (Eq. 5) needs to be corrected to improve average tint predictions.

Table 4. Prediction accuracy of the halftone model (Eq. 5) in CIE ΔE^*_{ab} with measured limits

	Uncoated Paper			Coated Paper		
	Average	Maximum	**Improvements**	Average	Maximum	**Improvements**
Cyan	1.90	3.78	0.04	1.72	3.48	-0.40
Magenta	3.25	9.65	0.61	3.25	6.46	-0.30
Yellow	2.46	5.14	0.03	2.78	8.9	0.05

3.3 Dot Segmentation into Solid ink and Mixed Area

The full dot was separated as solid dot and mixed area for an advanced analysis of color change within the ink region. The limiting TSVs for the paper (called limit-1) were the same as before, measured using 95% reference coverage, and the TSVs of the solid area comprising 3% reference ink were taken as the limit of the solid dots (called limit-2). Since the *xy*-coordinates of the mixed area frequently occupied the space between limit-1 and limit-2, these two limits were used to characterize the change of TSVs of the mixed area. This change is prominent for the magenta and yellow colorants in Fig. 6, which also shows that changes in the coordinates of solid inks were smaller, less scattered, and oriented more straightly than the full dots, as shown in Fig. 1. This means that the mixed area significantly affects the change of colorimetric values of a halftone image.

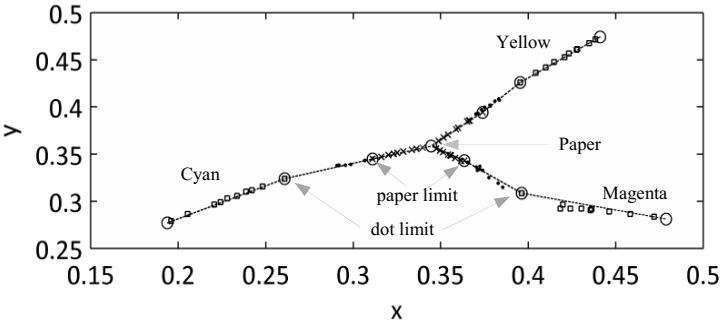

Fig. 6. CIE *xy*-chromaticity coordinates of solid ink (squares), mixed area (dots), the measured solid ink limit (circled square) and paper limit (circled cross)

In Eq. 3, T_{paper} was replaced by T_{limit1}, and T_{limit} by T_{limit2} to predict the changes of the mixed TSVs by fitting p to the measured data, as listed in Table 5 and illustrated in Fig. 7. For both coated and uncoated paper, the Y TSV in case of yellow colorants produced an unrepresentative value of p to reduce the number of ignorable rms errors. Therefore, in order to avoid misleading values, this particular p was replaced by the average p of X and Z TSVs. However, the average of X, Y, and Z exponents required to characterize the changes in the mixed area on coated paper ranged from 0.046 to 0.186 with an overall average of 0.106, and on uncoated paper from 0.069 to 0.334 with an average of 0.175. The low exponent value indicated small changes of color in the mixed area. The coated paper had smaller color variations in the mixed area because the ink spread and absorption was less than on uncoated paper. Therefore, the

exponent manifested the effect of ink spread and penetration properties of the halftone imaging system. Fig. 7 shows small changes of TSVs in mixed area and random variations in X for cyan or Y for magenta due to possible noise or measurement errors.

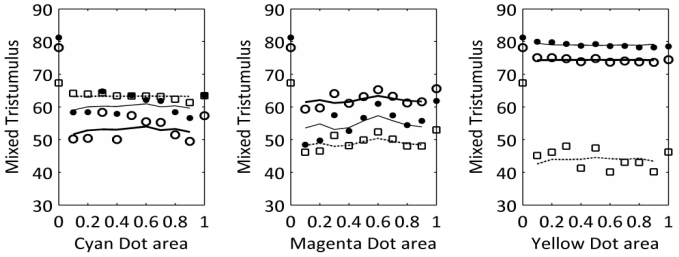

Fig. 7. Measured and predicted CIE TSVs X (circles), Y(dots), and Z (squares) of the mixed area as a function of printed area in coated paper. The lines represent the predicted values.

Table 5. Parameters of power function fittings for the dot and mixed TSVs (coated paper)

		Mixed area					Solid dots			
		T_{limit1}-T_{limit2}	T_{limit1}	*p*	*rms* error		T_{limit2} -T_{solid}	T_{limit2}	*p*	*rms* error
Cyan	X	18.51	57.34	0.110	2.95		19.94	38.83	0.792	1.91
	Y	15.33	63.56	0.105	2.48		21.22	48.22	0.838	1.97
	Z	1.61	63.43	0.043	0.87		10.24	61.82	1.13	0.84
Magenta	X	9.30	65.58	0.186	1.62		16.85	56.28	0.612	1.76
	Y	18.06	61.85	0.195	3.20		20.64	43.78	0.519	2.32
	Z	11.00	52.94	0.178	1.71		22.17	41.93	0.650	2.17
Yellow	X	1.96	74.49	0.024	0.58		3.70	72.53	0.696	0.23
	Y	0.45	78.54	0.046	0.54		4.11	78.08	0.776	0.24
	Z	13.41	46.17	0.068	2.85		19.56	32.75	0.636	1.06

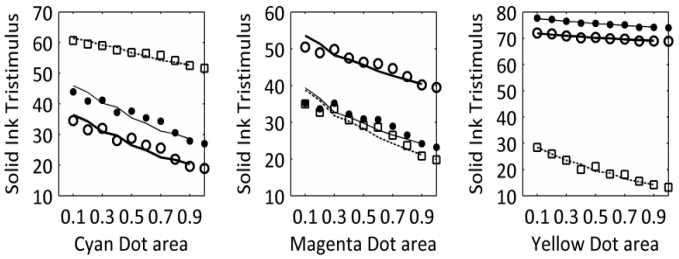

Fig. 8. Measured and predicted CIE X (circles), Y(dots), and Z (squares) TSVs of solid ink on coated paper. The lines represent the predicted values.

The average solid dot exponents required to account for light scattering on coated paper were ranged from 0.593 to 0.920 with an overall average of 0.738, and on uncoated paper ranged from 0.622 to 0.700 with an average of 0.655. Thus, the recorded

values were comparable to the values of exponents of the paper between the dots in order to correlate the effect of the light spread function and the halftone cell frequency. For example, a higher dot exponent for coated paper was because of the higher screen frequency of 175 *lpi*. Fig. 8 shows that the characterization performance of solid ink TSVs change was also convincing.

The halftone tint prediction accuracy, evaluated by Eq. 6, which also includes the effect due to the mixed area [6], is shown in Fig. 9 and listed in Table 6. The average accuracy for both coated and uncoated papers was identical at 1.53 ΔE^*_{ab}. Except for cyan on coated paper, all other ink-paper combinations recorded better prediction accuracies than the values in Table 2. The highest improvement was 2.64 ΔE^*_{ab} and the global improvement was slightly higher than $1\Delta E^*_{ab}$.

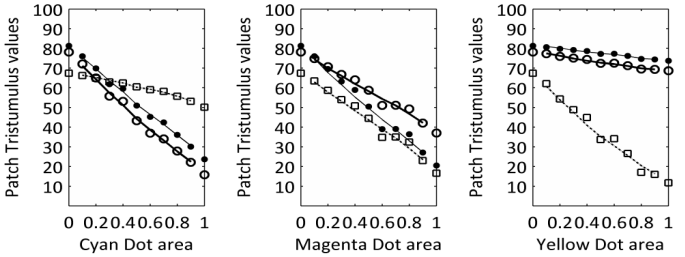

Fig. 9. Measured and predicted CIE TSVs X (circles), Y(dots), and Z (squares) of halftone patches in coated paper. The lines represent the predicted values.

Table 6. CIE ΔE^*_{ab} of the extended MD model (Eq. 6) that includes the effect of mixed area

	Uncoated Paper			Coated Paper		
	Average	Maximum	**Improvements**	Average	Maximum	**Improvements**
Cyan	1.76	2.96	0.18	1.56	3.08	-0.24
Magenta	1.22	3.29	2.64	1.75	4.71	1.20
Yellow	1.62	2.92	0.87	1.29	2.94	1.54

4 Conclusions

The change of colorimetric values of the halftone dots was larger than the paper between the dots for the electroink printing technology. The color of the dots or the paper between the dots was a mixture of colorimetric values of fulltone ink or base paper, respectively, and a limiting value. The simulated common limit used for characterizing the changes did not match with the measured limit. The measured distinct limits for the paper and the dots produced better characterization accuracy than a numerically calculated limit. However, the only empirical parameter – the model exponent – captured light scatter in the paper between the dots, but high values for the dots were not appropriate to explain the cause and effect. Nevertheless, the characterization of the dot area segmented into solid and mixed areas produced exponents comparable to the paper exponents. Notably, the low exponent value indicated small

changes of color in the mixed area as a function of printed coverage. Thus, the corresponding exponent manifested variation in ink thickness due to ink spreading and penetration of the halftone imaging system. In general, the empirical model parameter was a function of paper properties, inks, and halftone screen frequency.

A modified MD halftone equation to incorporate the variable colorimetry of the dots and the paper produced overall tint prediction accuracy ranging from 1.32 to 3.86 with an average of 2.56 CIE ΔE^*_{ab} using a theoretical limit. Although the use of measured limits improved characterizations of paper or the dot TSVs, the overall tint prediction accuracy was not significant. However, linearly adding the effect due to the mixed area in an expanded MD model yielded accuracy values ranging from 1.22 to 1.76 with an average of 1.53 ΔE^*_{ab}. The overall gain was more than 1 ΔE^*_{ab}. Therefore, segmenting the inked area into solid ink and mixed area generates more accurate predictions and better explanations of observed color changes.

This study showed that an expanded MD equation that follows the law of conservation of energy can predict halftone tints with satisfactory accuracy. Therefore, incorporating the concepts of dot area fragmentation, the change of paper and dot reflectance variations in the Neugebauer equations, for instance, should yield better prediction accuracy for color halftone prints. Testing these concepts for multicolor halftone images and rendering them practically useful require a simple method based on traditionally measured reflectance values.

Acknowledgements. EU Marie Curie Initial Training Networks (ITN) N-290154 (CP7.0) supported this research. We would like to thank Prof. Markku H. Kasari of University of Eastern Finland for providing advanced color measurement devices for this study.

References

1. Hébert, M., Hersch, R.D.: Review of spectral reflectance models for halftone prints: Principles, Calibration, and Prediction accuracy. COLOR Research and Application (2014), doi: 10.1002/col.21907
2. Wyble, D.R., Berns, R.S.: A Critical Review of Spectral Models Applied to Binary Color Printing. COLOR Research and Application **25**(1), 4–19 (2000)
3. Lewandowski, A., Ludl, M., Byrne, G., Dor, G.: Applying the Yule-Nielsen equation with negative n. J. Opt. Soc. Am. **23**, 1827–1834 (2006)
4. Arney, J.S., Engeldrum, P.G., Zeng, H.: An expanded Murray-Davies model of tone reproduction in halftone imaging. J. of Imaging Sci. Technol. **39**(6), 502–508 (1995)
5. Engeldrum, P.G.: The Color between the Dots. J. of Imaging Sci. Technol. **38**(6), 545 (1994)
6. Rahaman, G.M.A., Norberg, O., Edström, P.: Extension of Murray-Davies tone reproduction model by adding edge effect of halftone dots. In: Proc. SPIE 9018: 90180F (2014)
7. Arifin, A.Z., Asano, A.: Image segmentation by histogram thresholding using hierarchical cluster analysis. Elsevier Pattern Recognition Letter **27**(13), 1515 (2006)
8. Demirkaya, O., Asyali, M.H.: Determination of image bimodality thresholds for different intensity distributions. Elsevier Signal Processing: Image Communication **19**(6), 507 (2004)
9. Otsu, N.: A threshold selection method from gray-level histograms. IEEE Trans. Systems, Man and Cybernetics **9**, 62 (1979)